PERGAMON

International Journal of Heat and Mass Transfer 45 (2002) 3897–3910

International Journal of HEAT and MASS TRANSFER

www.elsevier.com/locate/ijhmt

Internal flow structure description of slug flow-pattern in a horizontal pipe

S. Lewis, W.L. Fu, G. Kojasoy *

Department of Mechanical Engineering, University of Wisconsin—Milwaukee, EMS Building, P.O. Box 784, 3200 N Cramer Street, Milwaukee, WI 53201, USA

Received 26 April 2001; received in revised form 9 March 2002

Abstract

Utility of the hot-film anemometry technique in describing the internal flow structure of a horizontal slug flow-pattern is discussed within the scope of intermittent nature of slug flow. It is shown that a single probe can be used for identifying the gas and liquid phases and for differentiating the large elongated bubble group from the small bubbles present in the liquid slug. Analyzing the nature of voltage signals, a signal processing scheme is developed for measurements of time-averaged void fractions of small and large bubbles as well as for the measurements of local mean axial velocity and turbulent intensity in the liquid phase. Some results of local measurements of time-averaged void fractions of small and large bubble groups, axial mean velocity and turbulent intensity are presented at relatively low and high gas and liquid flows for a horizontal slug flow-pattern in a 50.3 mm i.d. pipe.

Keywords: Slug flow; Void fraction; Hot-film anemometry

1. Introduction

The intermittent flow pattern, which are commonly defined as plug and slug flow, exists a wide-range of gas and liquid flow rates in a horizontal two-phase flow configuration. The plug flow-pattern is formed at very low gas velocities: it is characterized by elongated bubbles that move along the top of the pipe. At relatively high gas velocities for a given liquid flow a transition from plug to slug flow-pattern occurs. The slug flow is described by the intermittent appearance of aerated liquid slug occupying the entire cross-section, that are separated from one another by a large elongated gas bubble moving on top of a liquid layer. In order to advance the study of such a two phase flow structure, it is essential to experimentally obtain detailed local values of fundamental parameters, which can be used for phenomenologically based flow structure modeling.

The most significant and essential parameters for the plug/slug flow-pattern are the distribution of gas and liquid phases, the liquid velocity and its fluctuating components, the gas bubble and liquid transit frequency (or slug length), and the turbulent characteristics of interfacial transport of mass, momentum, and energy. These variables describe the local flow conditions of the quasi-steady slug flow, both qualitatively and quantitatively. Hence, accurate information about these parameters and relationships among them are necessary to understand the turbulent transport phenomena of the two-phase flow pattern.

A comprehensive physical model describing horizontal gas–liquid slug flow was first initiated by Dukler and Hubbard [1]. This model has been modified and extended over the years by Barnea and Brauner [2], Ruder et al. [3], Taitel and Barnea [4], Fabre and Line [5], Andreussi et al. [6] and Fan et al. [7] to apply to the entire intermittent flow-pattern and the slug flow transition. The predictive models developed by these investigators make it possible to obtain average liquid velocities both in the liquid slug and the liquid region underneath a large bubble, pressure drops, length of

* Corresponding author. Tel.: +1-414-229-5639; fax: +1-414-229-6958.

E-mail address: kojasoy@uwm.edu (G. Kojasoy).

0017-9310/02/$ - see front matter
PII: S0017-9310(02)00107-2

Nomenclature

A	cross-sectional area (m^2)
D	diameter of pipe (m)
j_f, j_g	local, time-averaged superficial velocities of liquid and gas
$\langle j_f \rangle$, $\langle j_g \rangle$	cross-sectional area-average value of j_f and j_g (m/s)
R	radius of pipe (m)
r	radial coordinate (m)
N_{lb}, N_{sb}	number of large and small bubbles (–)
t	time (s)
u	instantaneous axial velocity component (m/s)
u_{ave}	time-averaged local velocity (m/s)
u'	instantaneous local velocity fluctuation in axial direction (m/s)
$\overline{u'}$	root-mean-square values of u' (m/s)
u_{LS}	average liquid slug velocity (m/s)

Greek symbol

α	local void fraction

Subscripts

f	liquid phase
g	gaseous phase
lb	large bubble
sb	small bubble
sp	single-phase flow
tp	two-phase flow
LS	liquid slug

liquid slug, and slug frequencies, if the gas and liquid mass fluxes are provided. These models seem to give reasonable results when compared to experimental data of global measurements. However, these models cannot give the detailed void fraction distribution due to small and large bubbles, local velocity distribution, and the turbulent structure throughout the liquid phase. This information is of great importance to the eventual understanding and modeling of the basic hydrodynamics of two-phase slug flow. Due to the experimental difficulties associated with the intermittent nature of slug flow, very few detailed data have been reported in the literature. The problem of obtaining local data is complicated in horizontal flow configurations by the facts of axial asymmetry of the internal structure and that the slug flows do not exhibit a quasi-fully developed equilibrium condition.

Kvernvold et al. [8] used the combination of LDV and optical two-phase probes to measure the axial velocity distribution throughout a slug flow unit in a 24 mm i.d. horizontal tube of atmospheric pressure. Although the method gives good results at relatively low gas velocities the application of LDV induces technical difficulties in regions with high concentrations of small gas bubbles in the liquid slug occurring at higher gas flow rates. Andreussi et al. [6] successfully used local (optical) and cross-sectional (conductance) probes to measure the radial void fraction distribution in the liquid slugs, the size of the dispersed bubbles in the liquid slug and the aeration of the liquid layer underneath the slug bubble. Kawaji et al. [9] used the photochromatic dye activation technique to visualize the instantaneous motion of the liquid and gas slugs, and to successfully measure axial and vertical velocity profiles of the liquid phase in a horizontal slug flow. The experimental data were obtained for both circular and rectangular channels, and the liquid flow structure was found to be quite similar between the two channels. These previous studies have provided detailed basic information on the internal structure of the intermittent flow pattern in a horizontal configuration. However, issues associated with the local void fraction contributions due to elongated large bubbles and small bubbles, the turbulent structure, and interactions between dispersed and continuous phases are not addressed in these previous studies. Accurate prediction of flow requires detailed understanding of the local instantaneous interactions between continuous and dispersed phase. The horizontal slug flow-pattern introduces additional challenges because the dispersed phase by itself can only be characterized by two internal length scales and the velocity scales-one due to small bubbles in the liquid slugs and another associated with the large bubbles between two liquid slugs. Due to the complexity of interactions between dispersed and continuous phases and among dispersed phase bubbles, experimental approach remains fundamental in their analysis.

In view of the above discussion, it is evident that much experimental work is still necessary to attain a thorough physical understanding of the internal structure of an intermittent two-phase slug flow-pattern. In this context, an experimental investigation has been underway at the University of Wisconsin—Milwaukee to obtain local void fraction and velocity distributions and to clarify the turbulence structure of this flow pattern. In these experiments it is shown that the hot-film anemometry method can be used

- to identify liquid and gas phases, i.e., phase separation,

- to measure the local time-averaged void fractions due to large and small bubbles,
- to construct the local time-averaged, liquid velocity and turbulent intensity distributions,
- to investigate the dependence of the these parameters on the gas and liquid flow for an air–water intermittent flow in a 50.3 mm i.d. horizontal channel.

In the following, the hot film probe method, proper signal processing technique and the test facility are described, and based on the data, results are documented in terms of the local velocity, turbulent structure and void fraction distributions.

2. Hot-film anemometry method

2.1. Measurement principle

Hsu et al. [10] was the first to initiate the possible application of the hot-film anemometry technique to water–steam two-phase flows to identify the flow patterns and to measure the void fraction in an upward vertical flow channel. The probe temperature was raised above the saturation temperature of the water to induce nucleate boiling on the sensor. This allowed more sensitive measurements of the phase change, but removed the capability of measuring velocities. Delhaye [11] studied the response of hot-wire and hot-film probes in a liquid–gas two-phase flow. He found that although the hot-wire probes have given satisfactory results in measuring velocities and turbulence in single-phase flows, their fragility makes them impractical for two-phase flow measurements. The design is susceptible to the formation of deposits and the collection of debris on the sensor. In addition, the hot-wire probe is not electrically insulated from the surroundings and, therefore, large eddy currents could cause a signal shift. The hot-film probe relieves the problem of durability by replacing the wire with a thin film on the surface of a strong quartz rod. Delhaye [11] showed that local measurements of void fraction, liquid velocity and turbulence intensity in the liquid phase could be achieved by a proper use of the hot-film anemometry in air–water flows.

Since then, this technique has been used by Serizawa et al. [12], Abel and Resch [13], Wang et al. [14,15], Liu and Bankoff [16,17], Lance and Bataille [18] and Roig et al. [19] for describing the internal turbulence structure and phase distributions in vertical bubbly flow patterns. Theofaneous and Sullivan [20] demonstrated the utility of LDV to measure the turbulence structure in bubbly two-phase flow. Recently, Suzanne et al. [21] examined the application of LDV and hot-film anemometry methods for the liquid field velocity and void fraction measurements in plane bubbly mixing layer in vertical configurations. They concluded that at relatively higher void fractions (>2%), the LDV signal was no longer suitable because of the increase of the beam interruption rate by the bubble crossing. In this case, use of hot-film anemometry method was recommended. The utility of hot-film probes, particularly in relatively high-void fraction, provided information on the basic characteristics of bubbly flow in vertical configurations. However, only limited efforts were made to examine two-phase flow characteristics in large-scale experiments of the slug flow-pattern.

In principle, the hot-film anemometry method consists of the instantaneous measurement of the change in heat transfer from an electrically heated sensor. As the fluid flows past the constant temperature hot-film probe, changes in the fluid velocity, including turbulent fluctuations, cools the sensor at different rates. These changes in cooling rates result in voltage changes in the anemometer. In the case of an air–water two phase flow, the heat transfer rate between the two fluids is dramatically different. This results in abrupt voltage changes as the probe encounters phase interfaces. A typical sensor output for a horizontal two-phase slug flow is illustrated in Fig. 1. In order to illustrate the peculiarity of the hot-film probe signals in a horizontal slug flow the signals appearing in Fig. 1 were recorded simultaneously by two probes, one located at the upper portion of the pipe ($r/R = 0.8$) while the other located well below the passing large elongated bubbles.

As seen in Fig. 1a, when the probe is located in the upper portion of the pipe the sensor encounters the bubbles dispersed in the liquid slug. After the sharp initial drop, caused by the probe piercing the nose of a large bubble, the voltage gradually continues to decrease

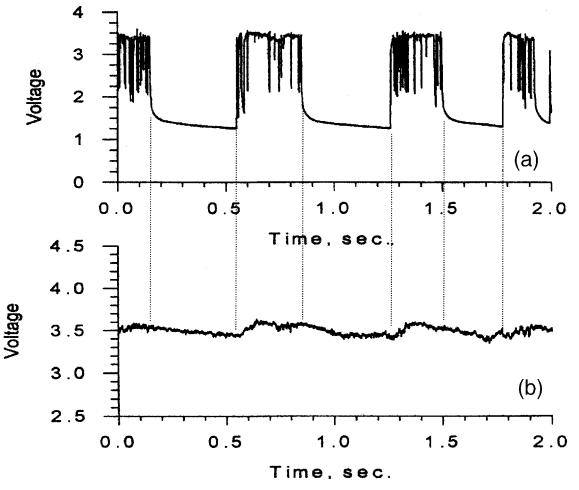

Fig. 1. Typical probe signals of two-probe measurements for $\langle j_f \rangle = 2.2$ m/s and $\langle j_g \rangle = 1.1$ m/s: (a) probe pierces through elongated large bubbles at $r/R = 0.8$, (b) probe located in liquid layer below passing large bubbles.

while the sensor is inside the gas bubble. This gradual decrease is due to the evaporation of a thin film of liquid that remains on the sensor. The probe is wetted immediately upon exiting the bubble, and the output signal from the probe shows a sharp increase to the previous level as it enters the liquid slug. When encountering a small gas bubble, in the liquid slug, the signal shows a sharp drop followed immediately by a sharp increase. These small bubble signals are quite different from those of large bubbles since the residence time in a small bubble is much shorter than those in a large bubble. On the other hand, the probe does not encounter any small bubbles when it is positioned in the lower portion of the pipe (Fig. 1b). In this case, the voltage signal shows an overall irregular wave motion believed to be caused by the passage of large bubbles over the top of the probe.

2.2. Signal processing

2.2.1. Phase identification

To process the anemometer voltage signal output for calculating the time-averaged void fraction and the flow field parameters, such as the time-averaged liquid phase mean velocity and turbulence intensity, the gas and liquid phases must be distinguished form each other and phase signals must be separated. Since the liquid and gas phases have significantly different heat transfer characteristics, the power required to maintain the probe temperature in each phase would be significantly different. Based on the drastic voltage change from one phase to another a number of methods have been developed. These methods have either analyzed the pure analog output from the probe or post-processed a digital record of this output. In both cases, however, the methods basically consisted of detecting the voltage changes associated with a change in phase.

Delhaye [11] used the method of classifying the voltage signals according to amplitude. He then related the void fraction to the areas of distribution in the amplitude histogram. Abel and Resch [13] proposed a method of using the digital output. Their method consisted of comparing each pair of successive voltage increases and decreases against predetermined liquid level threshold values. With this method the data had to be processed several times in order to determine the correct threshold values. These threshold values, therefore, were only valid for that particular data set. This method worked successfully for identifying the large bubbles. A second method was suggested for identifying the small bubbles.

In the present study Lance and Bataille [18] method, which was devised for a very low void fraction vertical bubbly flow, is modified for the intermittent flow-pattern for distinguishing phases. In this method signal processing is not only applied to the hot-film voltage $e(t)$ but also to its derivative $(\partial e/\partial t)$. This method based on

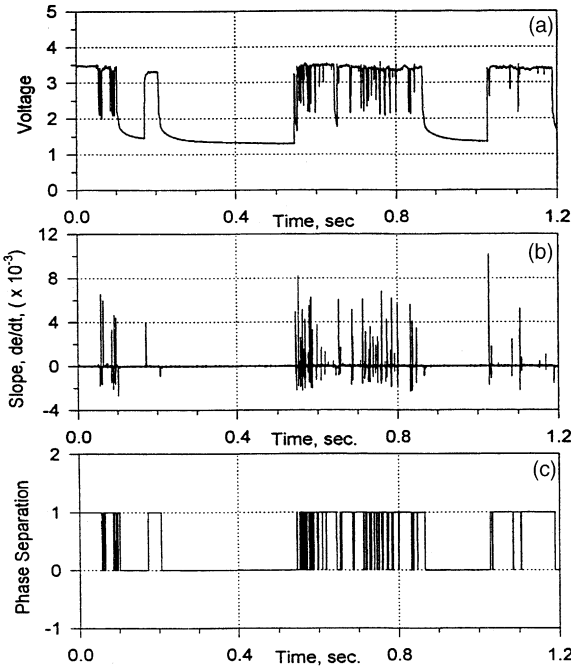

Fig. 2. Typical anemometer output and signal processing: (a) anemometer output signals, (b) slope of voltage signals, (c) phase separation step signals.

the derivative of the hot-film signal greatly magnifies the signals associated with the passage of bubbles and allow a better discrimination between bubbles and turbulence than a threshold method only applied to the signal $e(t)$. By plotting the anemometer voltage output and the slope on the same time scale (Fig. 2), effects of a bubble piercing the probe can be easily identified.

For each bubble passage, the slope signal shows a sharp negative spike for the nose of the bubble followed by a sharp positive spike for the tail of the bubble. Since the power required to heat the sensor to maintain its temperature in the gas phase is considerably less than in the liquid phase, the signal shows a decrease in the power to the sensor as a bubble is pierced by the probe. This decrease is responsible for the negative spike in the slope signal. Similarly, the positive spike in the voltage output slope is induced by a sharp increase in power required by the liquid phase. At this point, it is a matter of determining the proper threshold values to detect the spikes in the slope signal.

It is important to note that to accurately detect the gas bubbles, the threshold must also distinguish between the peaks induced by the probe sensor entering gas bubbles and those caused by the turbulent fluctuations in the liquid phase. By plotting the anemometer output voltage data and the corresponding slope as seen in Fig. 2 for the experimental data covering the entire range of gas and liquid flow rates, three threshold slope values

were identified. The first one is set as an indicator for the arrival of the gas phase at the probe sensor whereas the second one is used for determining the transition back to the liquid phase. The third threshold is needed to distinguish the turbulent fluctuations from the phase identification thresholds. The slope threshold is simply a scale in terms of two consecutive samples of voltage difference. For a fixed sampling rate each slope threshold value can be fixed satisfying all of the flow conditions. However, it is well known that the anemometer responds with a different level of liquid voltage signal for different flow conditions. Therefore, before processing a particular data set the level threshold value should be determined. Since a combination of the level and a series of slope thresholds are used in the present studies, it was not necessary to restrict the setting of level threshold to a value very close to the liquid signal.

Once the first slope threshold value is reached or exceeded on the negative plane, the phase separation step signal, δ; is set equal to unity, indicating the gas phase as shown in Fig. 2c. Once the slope signal exceeds the second threshold following the first one, the tail of the bubble is detected. However, the third threshold is also used to delay the detection of the liquid phase until the slope value decreases to the magnitude of the liquid phase turbulence threshold value. This indicates that the probe has fully reentered the liquid phase, and the phase separation signal, δ, is assigned a value of zero as observed in Fig. 2c.

The maximum time derivative of the signal induced by turbulence in the continuous phase remains very low in comparison with the time derivative associated with bubble when the gas–liquid interface impacts the hot-film sensor. However, this discrimination sometimes becomes difficult, especially for high void-fraction bubbly flow as observed by Suzanne et al. [21]. It is also the case when a high turbulent level is associated with a non-uniform bubble size distribution because the passage of small bubbles can be mistaken with turbulent fluctuations. Thus, the sampling frequency must be high enough in order to provide satisfactory information about whether the probe is located in liquid or in gas. In the present experiments conical type probes of TSI model 1231W was used, and after preliminary sensitivity studies the sampling frequency was optimized to be 5 kHz level. This frequency was much higher than the liquid turbulence frequency and allowed a statistically meaningful sampling time.

2.2.2. Separation of large and small gas bubbles

The second part of the phase discrimination process is to distinguish the elongated large bubbles from the small bubble group concentrated in liquid slugs. Only then the void fraction can be divided into contributions from small and large bubble groups, which is essential for understanding and modeling the local interfacial transport processes. The shape of elongated bubble being controlled by the tube diameter, their length is typically greater than a few pipe diameters. Thus, knowing their residence time and estimating their velocity would be useful for an objective criterion. However, the hot-film probe used in the present experiments is directed to measure the liquid velocity not the interfacial or gas velocities. There exist no satisfactory predictive methods for the elongated large bubble length. Furthermore, depending on the flow rates of each phase the size of each group varies requiring use of different criteria of the separation at each two-phase flow condition. We used the maximum small bubble chord-length, i.e., the maximum small bubble size, to differentiate the small bubbles signals from the elongated large bubble signals. Such an approach summarized below was enable us to determine a global threshold value that would be usable throughout the test matrix.

The phase separation signal gives the residence time for each bubble encountered. Then, when the residence time multiplied by a representative small bubble velocity yields the bubble chord-length. Here, the representative small bubble velocity in a liquid slug can be characterized by the liquid velocity, which is measured in the present experiments. This approach assumes a homogeneous two-phase flow model within the liquid slug, which is a good approximation for the horizontal slug flow configurations. The local measurements of liquid velocities are area-averaged from top of the tube to the maximum liquid velocity. This approximates the average velocity in the liquid slug where small bubbles mostly present. The maximum is found to be located at r/R of 0.1–0.2 but not below centerline for the entire range of experiments performed for the present study.

The averaged slug velocity is then used to approximately estimate the range of bubble chord-length, and hence, the small bubble sizes. A histogram is created to identify the bubble count and range of bubble chord-length by their respective residence time. An example of such histograms is illustrated in Fig. 3 for varying gas velocities at (a) $\langle j_f \rangle = 1.1$ m/s, (b) $\langle j_f \rangle = 1.65$ m/s, (c) $\langle j_f \rangle = 2.2$ m/s, where u_{LS} appearing on each figure refers to the average liquid slug velocity. From these figures the small bubble chord-length distribution is evident for varying gas and liquid superficial velocities. Due to presence of a few large bubbles in a given record, their location in the figure cannot be seen unless the time scale is drastically reduced.

Studying the small bubble size spectra figures and the visual observations made during each experimental conditions, a maximum threshold residence time is determined that would separate the large bubbles from the small bubble group. This characteristic residence time is ranged from 0.005 to 0.019 s for the entire range of present experiments. A global threshold residence time is set at 0.02 s. Such an approach of estimating a global

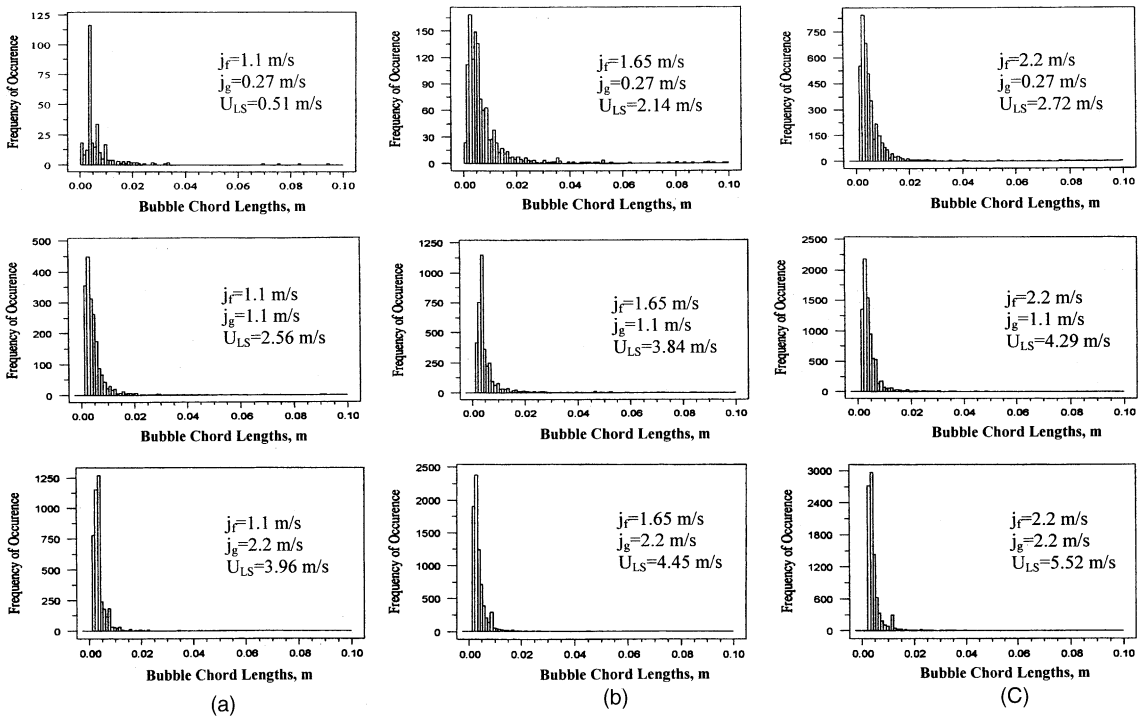

Fig. 3. Bubble size spectrum for varying gas velocities at (a) $\langle j_f \rangle = 1.1$ m/s and $\langle u_{LS} \rangle = 2.14$ m/s, (b) $\langle j_f \rangle = 1.65$ m/s and $\langle u_{LS} \rangle = 3.84$ m/s, (c) $\langle j_f \rangle = 2.2$ m/s and $\langle u_{LS} \rangle = 4.45$ m/s.

threshold bubble chord-length or residence time was necessary since at each experimental condition the average liquid slug velocity was not available until after the probe signal is analyzed by the signal processing scheme developed in this study. When the entire conditioned signals have been analyzed as described above, the data processing returns the phase separation signal. This signal is used to remove the liquid-phase data for analysis of velocity and turbulence in the liquid phase and the gas-phase data for void fraction analysis.

The local void fraction, $\alpha(r)$, at any probe location, r, can be obtained by the gas-phase data of hot-film probe sensor. It is defined as the local time-averaged void fraction by

$$\alpha(r) \equiv \lim_{T\to\infty} \int_0^T \delta(r,t)\,\mathrm{d}t \tag{1}$$

where δ, as a function of the space coordinate, r, and time, t, is equal to 1 if the probe sensor is in the gas phase and δ is equal to 0 if the sensor is in the liquid phase. As the signal is given in discrete form, Eq. (1) can be written as follows:

$$\alpha(r) \equiv \frac{1}{T}\sum_{m=1}^{N}(t_{2m} - t_{2m-1}) \tag{2}$$

where T is the total sampling time, N is the number of bubbles in the sample, t_{2m-1} is the time when the probe sensor enters into a bubble, and t_{2m} is the time the sensor enters into the liquid phase. Since the characteristic signal can be split into the large elongated bubble and small bubble group contributions, the void fractions for each bubble group are distinguished by classifying each bubble either in the large or small bubble group as follows:

$$\alpha(r) \equiv \frac{1}{T}\left[\sum_{i=1}^{N_{lb}}(t_{2i} - t_{2i-1})_{lb} + \sum_{j=1}^{N_{sb}}(t_{2j} - t_{2j-1})_{sb}\right] \tag{3}$$

where t_{2j-1} is the time when the probe sensor enters into the small bubble, and t_{2j} is the time the sensor enters into the liquid phase. Similarly, the subscript i identifies large elongated slug bubbles. N_{lb} and N_{sb}, respectively, are the number of large and small bubbles passing the probe sensor in the total sampling time, T. It is to be noted that

$$i = 1, \ldots, N_{lb} \quad \text{for large bubble group} \tag{4}$$

and

$$j = 1, \ldots, N_{sb} \quad \text{for small bubble group} \tag{5}$$

It is important to note that the void fraction, $\alpha(r)$ appearing in Eq. (3) is the total void fraction at a location r, which consists of the large bubble group defined by

$$\alpha_{lb}(r) \equiv \frac{1}{T}\sum_{i=1}^{N_{lb}}(t_{2i} - t_{2i-1}) \tag{6}$$

and the small bubble group defined by

$$\alpha_{sb}(r) \equiv \frac{1}{T}\sum_{j=1}^{N_{sb}}(t_{2j} - t_{2j-1}) \tag{7}$$

In view of Eqs. (3), (6) and (7), it is evident that

$$\alpha(r) \equiv \alpha_{lb}(r) + \alpha_{sb}(r) \tag{8}$$

It is to be noted here that both the small bubble and large bubble void fraction contributions are defined as the time-averaged void fraction based on the total sampling time T. There may be other forms of definitions in terms of weighting factors associated with the occurrence of each group. However, the way it is defined here makes more physical sense in terms of the unit-cell concept which has been frequently used in modeling the slug flow.

2.2.3. Liquid velocity field

After phase separation algorithm was performed to identify phases and to calculate the local time-averaged void fraction, the gas-phase data is taken away and the liquid-phase data is analyzed further for the local time-averaged axial velocity and turbulent intensity evaluations. The time-averaged velocity $u_{ave}(r)$ is given by

$$u_{ave}(r) = \frac{\left[\sum_{i=1}^{N} u_i(r,t)\right]}{N} \tag{9}$$

where $u_i(r,t)$ is the instantaneous liquid velocity, and N is the total number of discrete data points in the liquid phase.

As it was shown in a great detail by Sharma et al. [22], where two hot-film probes were used simultaneously to investigate the intermittent and transient characteristics of the slug flow-pattern, there exist short transition zones within liquid slugs right behind and ahead of large bubbles causing temporal variations on the mean velocity. In the mean time as it is observed in Fig. 1b, within the liquid layer below a passing large bubble, the velocity gradually decelerates from the large bubble nose. However, right before the large bubble tail a rapid acceleration is observed toward the wake region. An example of these observations at a probe location of $r/R = -0.6$ is illustrated in Fig. 4 for the case of $\langle j_f \rangle = 1.65$ m/s and $\langle j_g \rangle = 0.55$ m/s. The experimental data shown in this figure was obtained by simultaneous use of two hot-film probes. One of the probes was held at a fixed position $r/R = 0.8$ throughout the experiment while the other probe was traced through the vertical axis of the pipe, stopping at 18 positions to take measurements. With this arrangement of two probes, the local, instantaneous liquid velocity was measured at each location by the bottom probe, and the top probe was exclusively used to determine whether the bottom probe was in the liquid slug or in the liquid film underneath passing large bubbles. Since liquid slug length

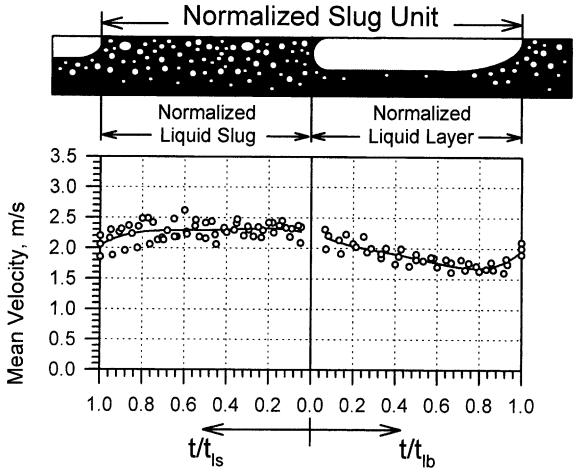

Fig. 4. Axial velocity variation in the liquid slug and the liquid layer under passing large bubbles.

and the length of large bubbles vary even at a given flow conditions, the time variation within the liquid slug is normalized by the liquid slug passage time, t_{ls}, and within the liquid layer by the large bubble passage time, t_{lb}. The ever developing nature of the liquid layer flow and the relatively uniform behavior of the liquid slug flow are clearly demonstrated from Fig. 4.

In view of the above it is evident that the mean liquid flow in a unit cell of a slug flow, i.e., a large bubble plus a liquid slug highly aerated by small bubbles, undergoes a series of changes. Although not quantitatively, these changes repeat themselves qualitatively for the next unit slug cell indicating that such a two-phase flow-pattern is inherently unsteady with large variations of mean velocity at any given location. Therefore, the transient nature of this two-phase flow-pattern introduces problems in decomposing the velocity field into a time-averaged motion and a random fluctuation due to turbulence as follows:

$$u'(r,t) = u(r,t) - u_{ave}(r) \tag{10}$$

where $u'(r,t)$ is the instantaneous turbulent velocity fluctuating component. The root-mean-square values of turbulent velocity fluctuations calculated in a traditional way for separating the random from organized motion would be in grave error due to undeterministic motion linked to the movement of the large and small bubbles. A frequency-based filtering process would not correct the situation. Therefore, a time-domain filtering method is introduced to remove the apparent unsteadiness in the mean liquid motion. The idea is that the mean flow varies on a time scale much larger than the turbulent fluctuations. This requires a sampling time of much smaller than the period of the unsteadiness in the mean flow.

In the present study, at each local measurement location the liquid-phase data are divided into several blocks. Each data block is analyzed separately to ensure statistically stationary results. In this way, the time-dependent mean velocity field is removed from the signal of each block without loosing or changing the basic characteristics of the local turbulence. The root-mean-square values of the velocity fluctuations for each block are calculated by

$$\overline{u_k'}(r) = \left\{ \sum_{k=1}^{n_k} [u_k(r,t) - u_{\mathrm{ave},k}(r,t)]^2 / n_k \right\}^{1/2} \tag{11}$$

where $u_{\mathrm{ave,k}}(r,t)$ is the time-dependent mean velocity in the k'th block, and the n_k is the number of data points in the k'th block. Finally, the overall root-mean-square value at a given location is calculated by

$$\overline{u'}(r) = \left\{ \sum_{k=1}^{N_k} [n_k (\overline{u_k'})^2] \Big/ \sum_{k=1}^{N_k} n_k \right\}^{1/2} \tag{12}$$

where N_k is the number of blocks. As it was shown by Evans [23] such an approach is justified for homogeneous, isotropic turbulence, and in this case ensemble averages may be replaced by time averages.

3. Experimental setup and procedure

3.1. Experimental setup

A schematic diagram of the experimental flow system is shown in Fig. 5. The flow loop consists of a horizontal line of 50.3 mm i.d. and 15.4 m Pyrex glass tubings with pressure tabs installed between them. The flow loop is entirely transparent to allow for flow visualization, high-speed photography and cinematography.

The air and distilled water are used as the two-phase coupling fluids. The air to the test section is supplied from a high-pressure university central air system and filtered as it enters a 0.95 m^3 capacity, high-pressure storage tank. The pressure is then stepped down, and the air flow is regulated by valves in parallel. The air flow is re-filtered and measured by series of well-calibrated turbine flow meters before air enters the mixing chamber. The distilled water is stored in a 1.9 m^3 capacity storage tank which containing cooling coils to control the water temperature. It is pumped from the tank by a stainless steel centrifugal pump and regulated from 0% to 100% of the pump capacity by a transistor inverter. This temperature control is essential in minimizing the temperature drift of the hot-film sensor.

The water flow rate is measured by a series of paddlewheel flow meters assembled in a parallel configuration. The air enters the two-phase mixing chamber from a 90° vertical leg and injected axially into the water flow through a cylindrical porous media of 100 μm porosity to achieve a uniform mixing. The two-phase mixture from the test section is directed to an air–water separator. The air is then vented to atmosphere, whereas the water is returned to the water storage tank for re-circulation.

Six diaphragm type pressure transducers along with six U-tube monometers are used to measure the pressure drop. The pressure transducers have a natural frequency of 5 Hz, with a range of 0–34.4 kPa, and an accuracy of ±0.3% of the full scale. The pressure of the air at the location of the flow meter and the two-phase system pressure at the test section are both measured.

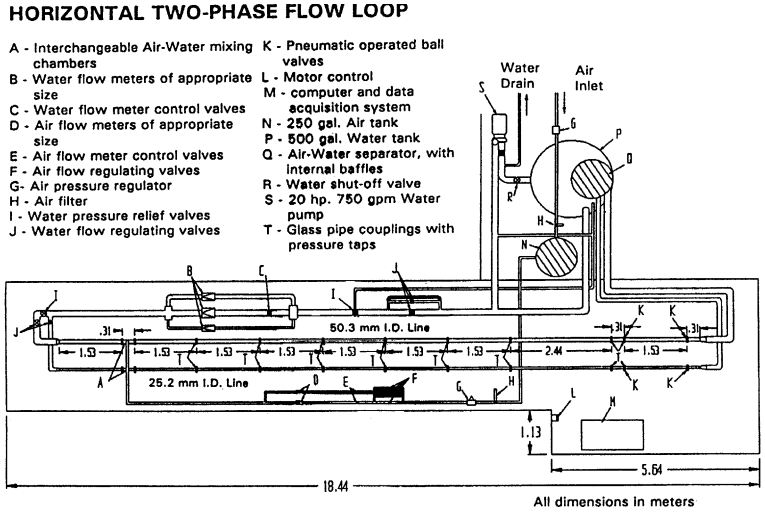

Fig. 5. Schematic of the experimental flow loop.

3.2. Experimental procedure

The experiments were carried out using hot-film anemometry and conical shaped (TSI 1231W) hot-film probes. The liquid and gas volumetric superficial velocities ranged from 1.1 to 2.2 and 0.27 to 2.2 m/s, respectively. For all the flow conditions, the system pressure was near atmospheric and the temperature about 20 °C.

A Vernier, with graduations to an accuracy of 0.01 mm, was used to traverse the probe in a direction perpendicular to the axis of the tube. The position of the probe was read on a digital linear scale. The high resolution was necessary to evaluate probe positions in the flow stream accurately and to ensure reproducible results. The hot-film probe was traced through the vertical axis of the pipe, stopping at 21 positions to take measurements.

Before beginning the two-phase measurements, single-phase liquid measurements were made to calibrate the instrumentation, verify their consistency with known results, and to serve as a reference for later comparison with two-phase flow measurements. The local mean axial velocity and the turbulent fluctuations in the axial direction were measured along the radial direction at $z/D = 253$ from the mixing chamber. The measured velocity profiles and turbulent fluctuations were non-dimensionalized with respect to the characteristic velocities of centerline velocity and friction velocity, respectively, for the purpose of comparing with Laufer's [24] benchmark data and Liu and Bankoff's [16,17] single-phase liquid flow data. The axial symmetry in fluctuations in $u_{ave}(r)$, and the root-mean-square values of the turbulent fluctuations, $u'(r)$, was found to be reasonably satisfied when compared with those results provided in these references.

The hot-film probe was calibrated in the single-phase liquid flow by comparing the sensor voltage level with the centerline velocity and fully developed turbulent flow pressure-drop information for each flow condition. The data was collected by the anemometer and stored into a computer. A FORTRAN program was used to process the data, separating the phases, converting the liquid phase voltage histogram to velocities, and calculating the essential parameters as described.

4. Experimental results and discussions

A sample of the time-averaged local void fraction, α, liquid phase mean axial velocity, u_{ave}, and the turbulence structure as presented by the turbulent intensity, defined as $\overline{u'}/u_{ave}$, are described in Fig. 6 for relatively low, medium and high values of $\langle j_g \rangle$ at a fixed value of $\langle j_f \rangle = 1.65$ m/s. Here, r/R is the normalized radial position of the hot-film sensor in the pipe, r, measured along the vertical axis from the pipe center to the probe, and R is the pipe radius. Thus, $r/R = -1.0$ and 1.0, respectively, identify the bottom and the top of the pipe. The single-phase liquid flow measurements of axial velocity and turbulence structure corresponding to the same liquid flow rates are also shown in these figures. When respective two-phase flow profiles are compared in these figures, it is evident that the void fraction, mean axial velocity, and turbulence structure distributions have similar behaviors. These results demonstrate interesting characteristics of a horizontal, slug flow pattern.

4.1. Void fraction profiles

As it is indicated by Eqs. (3) and (8), the void fraction measurement distinguishes the large bubble contributions from those of the small bubbles present in the liquid slug. Thus, the total void fraction is composed of these two contributions. The small bubble, large bubble and total void fraction distributions are illustrated in Fig. 6 for different $\langle j_g \rangle$ values.

It is evident from these figures that the void fraction distribution shows a sharp decrease toward the bottom of the pipe and practically becomes zero at a certain r/R location indicating the existence of a liquid layer free of voids. Visual observations showed that there are always some small bubble voids within the bottom liquid layer. However, the small bubble population is too small to be detected by the finite size probe. This liquid layer thickness, which is referred as the liquid film in the literature, decreases by increasing gas flow rates at a given liquid flow. It covers a liquid region below $r/R = -0.3$ at $\langle j_g \rangle = 0.55$ m/s and below $r/R = -0.6$ at $\langle j_g \rangle = 2.2$ m/s. This behavior points to the fact that small bubbles distribute more homogeneously as the gas flow increases.

The large bubble void fraction profile shows a sharp increase right after the liquid layer and then flattens gradually, going through a maximum, with a slight decrease toward the pipe wall. This decrease must be due to the interfacial curvature observed at the front and rear of a large bubble. The maximum, which moves downward as the gas flow rate increases, corresponds to the elongated large bubble nose position. On the other hand, the small bubble void fraction increases toward the top of the pipe indicating a strong small bubble migration toward the upper wall under the influence of gravitational segregation. Although the cumulative effect of small bubbles seems to be small, it drastically increases and becomes more homogeneously distributed with increasing gas flow as illustrated in Fig. 6. Considering the fact that the liquid slug length is much smaller than the gas slug length then it becomes obvious that the small bubble void fraction relative to the liquid slug volume may become extremely large at high gas flow rates.

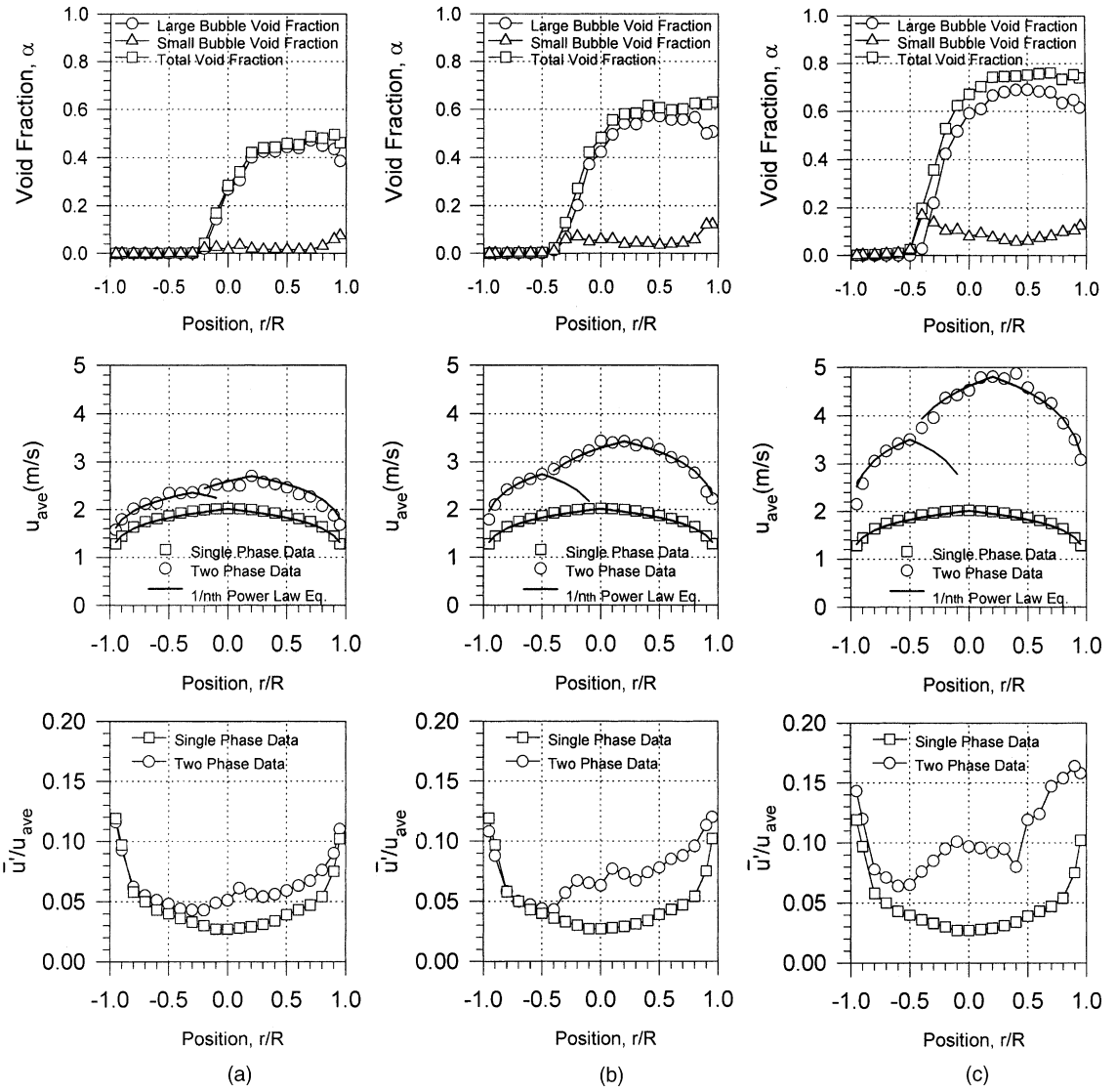

Fig. 6. Local void fraction, mean velocity and turbulence structure distributions (a) $\langle j_f \rangle = 1.65$ m/s and $\langle j_g \rangle = 0.55$ m/s, (b) $\langle j_f \rangle = 1.65$ m/s and $\langle j_g \rangle = 1.1$ m/s, (c) $\langle j_f \rangle = 1.65$ m/s and $\langle j_g \rangle = 2.2$ m/s.

4.2. Mean velocity profiles

The mean liquid velocity, u_{ave}, profiles illustrated in Fig. 6 show an asymmetric character of the liquid velocity profiles with the largest velocities located at the upper part of the pipe. The degree of asymmetry is shown to increase with increasing gas flows and seems to be well correlated with corresponding void fraction profiles. An interesting feature of the velocity distribution is that the profiles for all the cases exhibit a strong shear layer. When the velocity profiles are analyzed together with the void fraction distributions it is evident that the location of the shear layer corresponds well to the thickness of the respective liquid layer underneath the large bubble. Instantaneous velocity profiles, as measured by Kvernvold et al. [8], show a similar trend with regard to the appearance of the shear layer.

Another interesting feature of the velocity profile is that the velocity distribution within the bottom liquid layer exhibits a fully developed turbulent flow character as demonstrated by the $1/n'$th power law profile, which was fitted by the experimentally measured maximum velocity located in the liquid layer. Obviously, the maximum velocity profile in this liquid layer corresponds to the location where the void fraction nearly goes to zero. A similar fully developed turbulent velocity profile is

also observed within the liquid slug across the upper portion of the pipe. In this case, however, the maximum velocity in the liquid slug is used for fitting the $1/n'$th power law profile. The profiles shown in Fig. 6 have the same character as for fully developed turbulent flow profile with a transition zone from one to another. For the cases investigated during the course of present experiments we find that the area-averaged mixture superficial velocity is well correlated with the maximum liquid velocity. It is given by

$$\langle j_f \rangle + \langle j_g \rangle \cong (0.77\text{–}0.8) U_{max} \tag{13}$$

A kind of flow adjustment layer occurs between these two distinctive turbulent flow regions. This adjustment layer thickness decreases as the gas flow increases. In fact, the adjustment, or transition layer, is almost completely absorbed by the two turbulent profiles as shown in Fig. 6c, where the superficial gas velocity is much higher than the first two cases shown in Fig. 6a and b. This unique feature is somewhat similar to the recent observations of Kawaji et al. [9]. Even though, time-averaged, mean velocities are used here instead of the instantaneous velocity profiles presented by Kawaji et al. [9].

From the local values of $\alpha(r)$ and $u_{ave}(r)$ measured along the vertical axis, the area-averaged liquid superficial velocity $\langle j_f \rangle$ was calculated as follows:

$$\langle j_f \rangle \equiv \frac{1}{A} \int_A [1 - \alpha(r)] u_{ave}(r) \, dA \tag{14}$$

where A is the cross-sectional area of the pipe.

In order to check the accuracy of both local void fraction and the mean axial liquid velocity measurements, the area-averaged liquid superficial velocity calculated by Eq. (14) was compared with corresponding liquid superficial velocity as measured by the flow meter. It was observed that the calculated superficial velocity was consistently over-estimated by a margin of ±4.2–12%. There may be several reasons for such a consistency. First, as noted by Delhaye [11] and Wang et al. [14] the void fraction measured by the conical hot-film probe technique is underestimated due to the deformation and the deflection of the bubbles by the probe. Such an experimental error is expected to be more pronounced in measuring the small bubble contribution toward the total void fraction expressed by Eqs. (3) and (8). Secondly, as demonstrated by Fig. 1b, the data show a wavy pattern when the probe is located underneath the slug bubble. Although a correction on the time domain was performed to smooth out the behavior, this may still cause some errors in calculating the mean velocity in the liquid phase. Finally, the small-amplitude peaks due to incomplete piercing of small bubbles or due to the bubble sliding on the probe are difficult to detect by the present data processing scheme. This is again expected to be the case in the small bubble encounter of the probe. These series of experimental errors are probably the main causes of the systematic error observed in matching the liquid superficial velocities.

4.3. Turbulence structure

The turbulence structure is presented in Fig. 6 in terms of the turbulent intensity as defined by $\overline{u'}/u_{ave}$, where $\overline{u'}$ is the root-mean-square value of instantaneous local velocity fluctuation. Both the axial turbulent fluctuations and turbulent intensities generally increased toward the bottom wall and go through a minimum at the top edge of the bottom liquid layer. Furthermore, it is interesting to note that both profiles follow very closely to the corresponding single-phase flow turbulent fluctuations and intensities within the bottom liquid layer, which is practically free of voids as discussed above. As it is expected, the turbulence in this region is slightly enhanced by the passage of large bubbles. But it preserves the general character of single-phase flow turbulence intensity.

On the other hand, the turbulence drastically increases as the probe is moved away form the bottom liquid layer toward the bubbly liquid slug region, and reaches a local maximum at the maximum mean velocity level. In the core of the liquid slug, the turbulence stays nearly constant and shows a sharp increase toward the top wall. This enhanced turbulence might be related to the observed trend of small bubble void fraction profiles, which also shows a sharp increase toward the top of the pipe as shown in Fig. 6. Parallel to the mean velocity behavior, the local axial turbulence structure shows a two regions behavior, the liquid layer and bubbly liquid slug regions. This consistent tendency of turbulence points to the fact that the local turbulent motion is directly related to the local two-phase flow motion.

Probably not the most distinctive, but certainly the most surprising observation from Fig. 6 is the variation of turbulence intensity in the lower part of the pipe. A careful inspection of the first two figures in the lower part indicates that the turbulence intensity is slightly, but consistently, lower than the corresponding single-phase intensity. This phenomenon is observed only at relatively low gas and liquid flows. As discussed above with regard to the void fraction profiles, always there exist small bubbles in the lower part. However, the population and frequency of small bubbles are too small to detect with a finite size probe and, therefore, cannot be traceable in Fig. 6. It seems that the extremely small values of void fraction tend to lower the turbulence intensity. This is so-called "lubrication" effect of a very small bubble population was observed in vertical bubbly flow configuration by Serizawa et al. [12] and Wang et al. [15].

It is customary practice in vertical bubbly two-phase flow experiments to express the bubble-induced turbulence components as the difference between the

two-phase bubbly flow turbulence and the corresponding single-phase wall-generated components. Based on this type of superposition hypothesis, the enhanced two-phase flow fluctuation $\overline{u'}_{tp}$ can be expressed as the sum of the single-phase turbulence, $\overline{u'}_{sp}$, and the bubble-induced turbulence, $\Delta\overline{u'}$. Thus,

$$\overline{u'}_{tp} = \overline{u'}_{sp} + \Delta\overline{u'} \tag{15}$$

With this hypothesis the relative effect of bubble-induced turbulence in the axial direction can be calculated from the measured data of two-phase and corresponding single-phase flows. Results are shown in dimensionless form in Fig. 7. It is evident from this figure that the ratio of bubble-induced turbulence to the total turbulence strongly depends on the local flow conditions. Generally, this ratio increases with increasing gas flow, and follows very closely the two-layer velocity profile structures. The lubrication effect of very small bubble population is evident at relatively low gas flow of $\langle j_g \rangle = 0.27$ m/s. At relatively high gas flows, the bubble-induced turbulence contribution accounts for more than 80% of the total turbulence toward the top of the pipe where the void fraction is high. However, this generally increasing trend with the local void fraction distribution does not reflect the wall peaking void fraction as observed in Fig. 6. On the other hand, increasing the liquid flow at constant gas flow generally decreases the ratio of $\Delta\overline{u'}/\overline{u'}_{tp}$ within the liquid layer region and has a minimal effect in the high void fraction region above the liquid layer. This damping effect of liquid flow in vertical bubbly two-phase flow was also observed by Liu and Bankoff [16].

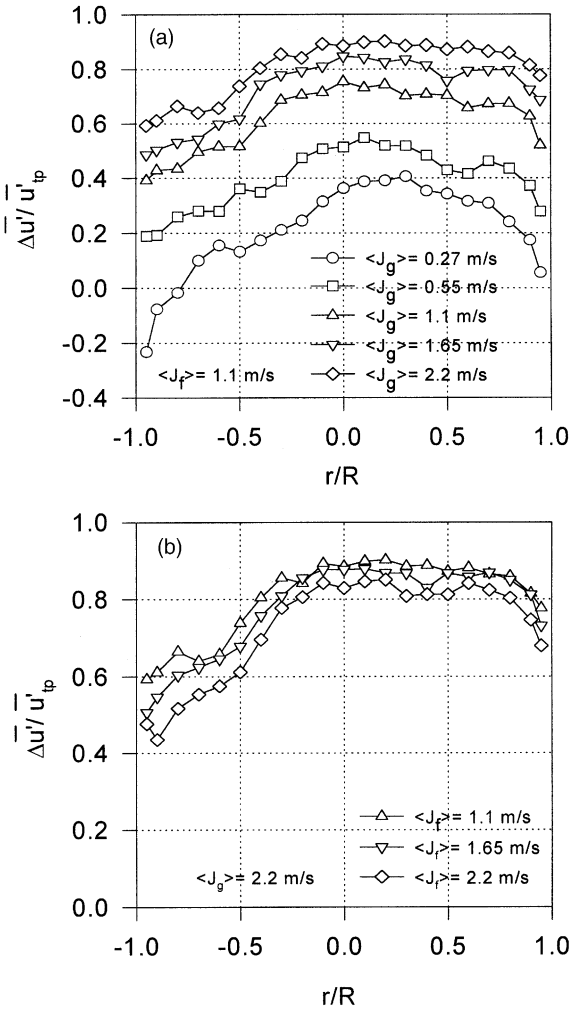

Fig. 7. Local variation of bubble-induced axial turbulence: (a) effect of gas flow at $\langle j_f \rangle = 1.1$ m/s (b) effect of liquid flow at $\langle j_g \rangle = 2.2$ m/s.

4.4. Effect of flow variables

The profiles of the local void fraction, liquid phase mean velocity and turbulent intensity are shown on Fig. 8a, for the case of an increasing gas flow rate at a constant value of the liquid flow. The large bubble void fraction drastically increases with increasing gas flow. An increase in the small bubble void fraction can also be noted. However, the bottom liquid layer thickness decrease with increasing gas flow. The introduction of gas into a water flow generally accelerates the velocities, with a relatively steeper increase at the upper portion of the pipe than in the liquid layer. As noted with regard to Fig. 6, a consistent shear layer appears on all the flow conditions at the same location, namely, where the void fraction profile goes to zero. With increasing gas flow, the slope of the mean velocity profile above the shear layer increases along with the overall magnitude. It is evident that the turbulence increases significantly upon increasing the gas flow. At the bottom liquid layer, the relative turbulence, as characterized by the local turbulent intensity, follows very closely the single-phase flow intensity. However, after the shear layer, the turbulence is strongly enhanced with the increasing gas flow. This enhancement may be attributed to the increased population of small bubbles in the liquid slug toward the top of the pipe.

The influence of increasing liquid flow at a constant flow is demonstrated in Fig. 8b. The effect of increasing liquid flow is to decrease the large bubble void fraction. However, the small bubble void fraction shows a sharp increase. This may be due to the increase in the local turbulence and interfacial instability both of which result in disintegration and generation of small bubbles. With increasing liquid flow, the mean velocity profile develops toward a symmetric behavior. The turbulent intensity in the bottom liquid layer is almost indistinguishable for a wide range of gas flow rate. On the other hand the axial turbulent intensity generally increased toward the wall and became flat in the core region. An

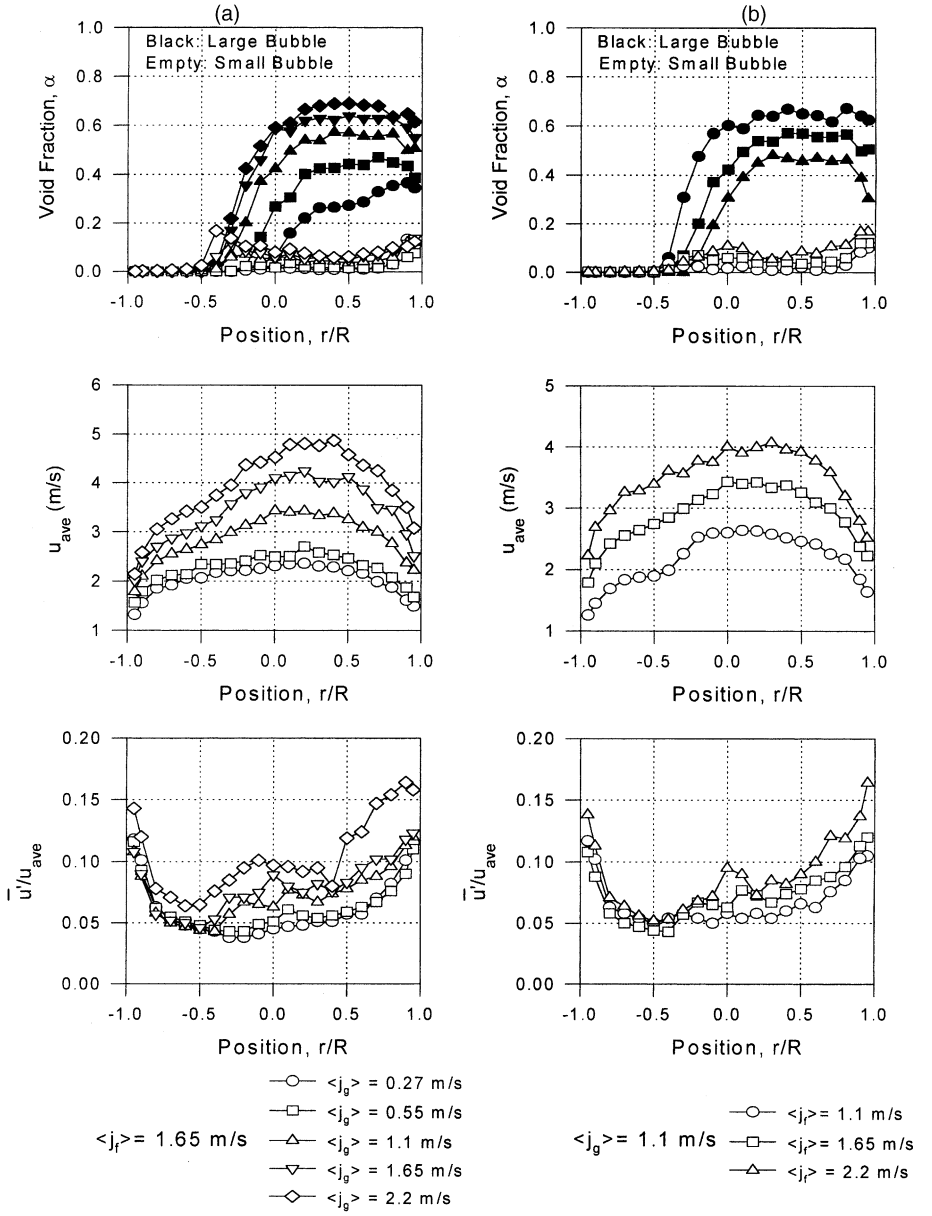

Fig. 8. Influence of gas and liquid flow on local distribution of void fraction, mean liquid velocity and turbulent intensity: (a) effect of gas flow at $\langle j_f \rangle = 1.65$ m/s, (b) effect of liquid flow at $\langle j_g \rangle = 1.1$ m/s.

interesting conclusion can be drawn when Fig. 7b is compared to Fig. 8b. Even though the absolute turbulence level is enhanced with the increasing liquid flow, the rate of increase of $\overline{u'}_{tp}$ is less than that of $\overline{u'}_{sp}$.

5. Summary and conclusions

It is demonstrated that the hot-film anemometry technique can be successfully utilized in a horizontal two-phase slug flow-pattern (a) to distinguish the gas and liquid phases, (b) to differentiate the large bubble group from the small bubble group present in the liquid slug, (c) to measure the time-averaged local void fractions of small and large bubble groups and (d) to measure the local axial mean velocity and turbulent intensity in the liquid phase.

The experimental results for a 50.3 mm i.d. horizontal slug flow indicate that the large bubble void fraction profile shows a sharp increase right after the

liquid layer and then flattens gradually, going through a maximum, with a slight decrease toward the pipe wall. On the other hand, the small bubble void fraction increases toward the top of the pipe indicating a strong small bubble migration toward the upper wall. It was found that increasing the gas flow at a fixed liquid flow would increase the local slug bubble void fraction.

The mean velocity profiles showed an asymmetric behavior with the largest velocities located at the upper part of the pipe. The degree of asymmetry was shown to increase with increasing gas flow. An interesting feature of the liquid velocity distribution is that the profiles, for all the cases studied, exhibited a strong shear layer starting at the top of the bottom liquid layer. The most interesting feature of the slug flow was that the bottom liquid layer and the top portion of the liquid slug tended toward a fully developed turbulent pipe-flow profile.

Increasing the gas flow rate, increased not only the absolute turbulence, but also the turbulent intensity over the whole cross-section. This effect of the gas superficial velocity was more pronounced within the liquid slug than the bottom liquid layer. In general, it was concluded that the local turbulence and the bubble-induced turbulence components were directly related to the main stream motion within the liquid phase.

Acknowledgements

The work reported in this paper was performed under the auspices of the US Department of Energy, Office of Basic Energy Science. The authors would like to express their sincere appreciation for the encouragement, support and technical comments on this program from Dr. R. Price and Dr. R. Goulard of the US DOE/BES.

References

[1] A.E. Dukler, M.G. Hubbard, A model for gas–liquid flow in horizontal and near horizontal tubes, Ind. Engng. Chem. Fundam. 14 (1975) 337–347.

[2] D. Barnea, N. Brauner, Holdup of the liquid slug in two-phase intermittent flow, Int. J. Multiphase Flow 11 (1985) 43–49.

[3] Z. Ruder, P.J. Hanratty, T.J. Hanratty, Necessary conditions for the existence of stable slugs, Int. J. Multiphase Flow 15 (1989) 209–226.

[4] Y. Taitel, D. Barnea, Two-phase slug flow, in: J.P. Hartnett, T.F. Irvine (Eds.), Advances in Heat Transfer, vol. 20, Academic Press, New York, 1990, pp. 83–132.

[5] J. Fabre, Line, Modeling of slug flow, in: J.L. Lamley, M. Van Dayke, H.L. Reed (Eds.), Ann. Rev. Fluid Mech. 24 (1992) 21–46, Ann. Rev. Inc.

[6] P. Andreussi, K.H. Bendiksen, O.J. Nydal, Void distribution in slug flow, Int. J. Multiphase Flow 19 (1993) 817–828.

[7] Z. Fan, F. Lusseyran, T.J. Hanratty, Initiation of slugs in horizontal gas–liquid flows, AIChE J. 39 (1993) 1742–1753.

[8] O. Kvernvold, V. Vindoy, T. Sontvedt, A. Saasen, S. Selmer-Olsen, Velocity distribution in horizontal slug flow, Int. J. Multiphase Flow 10 (1984) 441–457.

[9] M. Kawaji, M. Ali, A. Ciastek, C. Lorencez, Study of liquid flow structure in horizontal cocurrent gas–liquid slug flow, Proceedings of the ANS-THD 8, 1995 Natlional Heat Transfer Conference, August 5–9, Portland, Oregon, 1995, pp. 79–88.

[10] Y.Y. Hsu, F.F. Simon, R.W. Graham, Application of hot-wire anemometry for two-phase flow measurements such as void fraction and slip velocity, Proceedings of the ASME Winter Meeting, Philadelphia, PA, 1963.

[11] J.M. Delhaye, in: B.W. Le Tourneau, A.E. Bergles (Eds.), Hot-film Anemometry in Two-phase Flow, Two-phase Flow Instrumentation, ASME, New York, 1969, pp. 58–69.

[12] A. Serizawa, I. Kataoka, L. Michiyoshi, Turbulence structure of air–water bubbly flow. I. Measuring techniques, Int. J. Multiphase Flow 2 (1975) 221–233.

[13] R. Abel, F.J. Resch, A method for the analysis of hot film anemometer signals in two-phase flows, Int. J. Multiphase Flow 4 (1978) 523–533.

[14] S.K. Wang, S.J. Lee, O.C. Jones, R.T. Lahey, Local void fraction measurement techniques in two-phase bubbly flow using hot-film anemometry, Proceedings of the 22nd Heat Transfer Conference, Niagara Falls, August 5–8, 1984.

[15] S.K. Wang, S.J. Lee, O.C. Jones, R.T. Lahey, 3-D turbulence structure and phase distribution measurements in bubbly two-phase flows, Int. J. Multiphase Flow 8 (1987) 327–343.

[16] T.J. Liu, S.G. Bankoff, Structure of air–water bubbly flow in a vertical pipe. I. Liquid mean velocity and turbulence measurements, Int. J. Heat Mass Transfer 36 (1993) 1049–1060.

[17] T.J. Liu, S.G Bankoff, Structure of air–water bubbly flow in a vertical pipe. II. Void fraction bubble velocity and bubble size distributions, Int. J. Heat Mass Transfer 36 (1993) 1061–1072.

[18] M. Lance, J.M. Bataille, Turbulence in the liquid phase in a uniform bubbly air–water flow, J. Fluid Mech. 222 (1991) 95–118.

[19] V. Roig, C. Suzanne, L. Masbernat, Measurement in two-phase mixing layer, Third World Conf. Exp. Heat Trans., Fluid Mech Therm., Honolulu, Hawaii, 1993, pp. 1342–1348.

[20] T.G. Theofaneous, J. Sullivan, Turbulence in two-phase dispersed flows, J. Fluid Mech. 116 (1982) 343–362.

[21] C. Suzanne, K. Ellingsen, F. Risso, V. Roig, Local measurements in turbulent bubbly flows, Nucl. Eng. Des. 184 (1998) 319–327.

[22] S. Sharma, S. Lewis, G. Kojasoy, Local studies in horizontal gas–liquid slug flow, J. Nucl. Eng. Des. 184 (1998) 305–318.

[23] R.L. Evans, Turbulence and unsteadiness measurements downstream of a moving blade row, J. Eng. Power Trans. ASME (January 1975) 131–139.

[24] J. Laufer, The structure of turbulence in fullydeveloped pipe flow, NACA Rep. 1174 (1954).